Validation of the edge density profiles from the ICRF antenna reflectometer on ASDEX Upgrade Upgrade team and the EUROfusion MST1 team

Egor Seliunin, Carlos Silva, P. Manz, G D Conway, L. Gil, Stéphane Heuraux, T. Putterich, Antonio Silva, Filipe da Silva, Ulrich Stroth, et al.

Validation of the edge density profiles from the ICRF antenna reflectometer on ASDEX Upgrade

E. Seliunin,[a] C. Silva,[a] P. Manz,[b] G.D. Conway,[b] L. Gil,[a] S. Heuraux,[c] T. Pütterich,[b] A. Silva,[a] F. da Silva,[a] U. Stroth,[b,d] J. Vicente,[a] E. Wolfrum,[b] W. Zhang[b] and the ASDEX Upgrade team and the EUROfusion MST1 team[2]

[a] *Instituto de Plasmas e Fusão Nuclear, Instituto Superior Técnico, Universidade Lisboa, Av. Rovisco Pais 1, 1049-001 Lisboa, Portugal*

[b] *Max-Planck-Institut für Plasmaphysik, Boltzmannstr. 2, 85748 Garching, Germany*

[c] *Institut Jean Lamour UMR 7198 CNRS-Université de Lorraine, ARTEM BP 50840, F-54011 Nancy, France*

[d] *Physik-Department E28, Technische Universität München, 85747 Garching, Germany*

E-mail: egor.seliunin@tecnico.ulisboa.pt

Abstract: A new multichannel X-mode reflectometer diagnostic (RIC) was recently installed in ASDEX Upgrade (AUG) to provide the electron density profiles in front of an ion cyclotron range of frequencies antenna. The diagnostic was designed to measure density profiles up to 2×10^{19} m^{-3} in the typical 1.5–2.7 T magnetic fields of AUG. Profiles can be measured every 25 μs simultaneously in 3 different poloidal positions. The main objective of this work is to assess the measurement capabilities of the RIC diagnostic for the scrape-off layer density profiles. RIC density profiles are compared to radial profiles from lithium beam emission spectroscopy and Thomson scattering over a wide variety of plasma conditions. Although a good agreement between the different diagnostics is generally found at low discharge densities, RIC measurements often show steeper profiles at high discharge densities, particularly at low outer wall clearance. In addition, the location of the start of X-mode upper cutoff reflection is determined as well as the plasma density at the first cutoff layer.

Keywords: Nuclear instruments and methods for hot plasma diagnostics; Data processing methods

Contents

1 Introduction

A multichannel X-mode reflectometer diagnostic (RIC) was recently installed in the ASDEX Upgrade tokamak (AUG) inside the ion cyclotron range of frequencies antenna [1]. This system provides electron density profiles up to $2 \times 10^{19}\,\mathrm{m}^{-3}$ in the typical 1.5–2.7 T magnetic fields of AUG with a maximum repetition rate of one profile every 25 µs. Having the advantage of high temporal and spatial resolution, and unique possibility to measure electron density profiles simultaneously in three different poloidal positions (see figure 1, right), the system can provide relevant information for the characterization of the scrape-off layer (SOL).

The wave propagation for X-mode depends both on the plasma density and local magnetic field strength. The X-mode upper branch cutoff frequency reads

$$f_{\mathrm{UC}} = \sqrt{f_{\mathrm{pe}}^2 + f_{\mathrm{ce}}^2/4} + f_{\mathrm{ce}}/2, \tag{1.1}$$

where plasma frequency is proportional to electron density, $f_{\mathrm{pe}}^2 \propto n_e$, and electron cyclotron frequency is proportional to magnetic field, $f_{\mathrm{ce}} \propto B$ [2]. The initialization of density profiles measured by X-mode reflectometry is crucial for the profile reconstruction as it determines the location of the first measured density. The reconstructed profile initial location is determined by the probing frequency corresponding to the start of X-mode upper cutoff reflection (is also called First Fringe (FF) reflection), f_{FF} [3–6], and on the plasma density at the FF. The first reflection occurs close to zero density and becomes challenging to detect due to the low amplitude of the reflected signal and to the uncertainty about the plasma density at the first cutoff layer. Ideally, FF arises at $n_{\mathrm{e}} \to 0$, i.e. $f_{\mathrm{FF}}(= f_{\mathrm{UC}}) \approx f_{\mathrm{ce}}$. In reality, the f_{FF} is estimated at some density $n_e = n_{\mathrm{e},0} \neq 0$. This density is called residual density. Knowing $f_{\mathrm{FF}}(= f_{\mathrm{UC}})$, and assuming $n_{\mathrm{e},0}$, one can estimate the initial position of the density profile from the magnetic field profile [3, 4]. In this paper, the residual density and the position of the first reflection are studied aiming at validating RIC density profiles. In addition, we compare RIC profiles against lithium beam and Thomson scattering data for different experimental conditions.

2 Experimental set-up

The radial transport on the low-field-side (LFS) of tokamaks is strongly influenced by the outward propagation of field-aligned convective structures known as filaments [7]. At high discharge densities, a flattening of the SOL density profiles is observed to be associated with the enhancement of the radial transport due to a regime change of the filamentary transport when the Greenwald fraction, f_{GW}, overcomes certain value (for AUG typically $f_{\mathrm{GW}} \approx 0.45$–$0.5$) [8]. Here $f_{\mathrm{GW}} = \bar{n}_{\mathrm{e,core}}/n_{\mathrm{GW}}$, and the Greenwald density, $n_{\mathrm{GW}} = I_p/\pi a^2$ (where I_p and a are the plasma current and minor radius) [9]. Aiming at validating the edge density profiles measured by RIC, two discharges with different SOL transport regimes are selected.

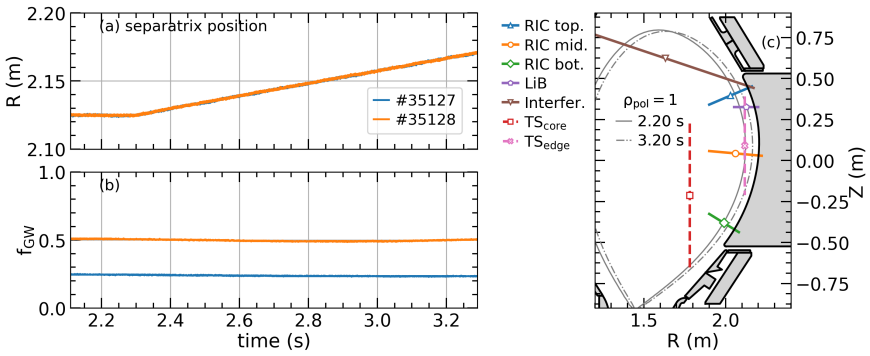

Figure 1. Left, temporal evolution of the separatrix radial location at the outer middle plane obtained from the magnetic reconstruction (a) together with Greenwald fraction (b) for discharges #35127 and #35128. Right (c), poloidal cross-section of AUG together with lines of sight of RIC, interferometer, LiB, edge and core TS diagnostics. The separatrix position is shown at the extremes of the outer wall clearance scan.

Two Ohmic heated discharges at $I_p = 0.8\,\mathrm{MA}$ with a scan in the outer wall clearance were performed at different Greenwald fractions: $f_{\mathrm{GW}} \approx 0.2$ (#35127, low density) and ≈ 0.5 (#35128, high density). The time traces of f_{GW} and radial position of the separatrix are shown in figure 1. A magnetic field of $B_t = -2.0\,\mathrm{T}$ (the negative direction of B_t is defined as the clockwise direction taking as reference the top view of the tokamak) was chosen to maximize the density range probed by RIC.

Due to memory constraints, RIC profiles cannot be stored at the maximum acquisition rate for the three antennas during the entire discharge. Therefore, the RIC profile acquisition rate was reduced to $40\,\mu\mathrm{s}$.

In addition to RIC, the SOL density profiles were also measured by lithium beam emission spectroscopy (LiB) [10], and edge and core Thomson scattering systems (TS) [11]. The lines of sight of the different diagnostics are shown in figure 1 together with a poloidal cross-section of AUG showing the separatrix position at the two extremes of the outer wall clearance scan.

3 Electron density profiles

RIC density profiles are reconstructed using Bottollier-Curtet's technique [12] in combination with a method similar to the burst-mode analysis in [13], as RIC data is optimized when 4 consecutive

Table 1. Radial shift of the density profiles (averaged over 50 ms) for the different diagnostics to match the edge interferometry density measurements in low (#35127, discharge 1) and high (#35128, discharge 2) density discharge. The positive/negative sign corresponds to an outward/inward shift of the profile.

	LiB (mm)		top. (mm)		mid. (mm)		bot. (mm)		core TS (mm)		edge TS (mm)	
time (s)\discharge	1	2	1	2	1	2	1	2	1	2	1	2
2.2	0	0	−4	−5	−3	−10	−8	−10	0	0	6	0
2.8	−6	0	0	−10	−2	−8	−6	−10	0	0	6	0
3.2	−8	0	3	6	−1	0	−1	0	0	0	6	0

sweeps are summed together [4]. The determination of profile initial location requires first fringe frequency, f_{FF}, and residual density, $n_{e,0}$ (see section 1). We estimate the f_{FF} by applying the algorithm described in [4, 5, 14] to a central moving average of a 100 sweeps. A threshold value $A_{threshold} = 0.1(\max(A) - \min(A)) + \min(A)$ is used to detect a rise in the signal amplitude (A) in a selected range of the probing frequencies from f_{ce} at the wall to f_{ce} at the separatrix. A constant $n_{e,0} = 10^{17}\,\mathrm{m}^{-3}$ is used for RIC profiles initialization (see section 4.2). The reconstructed RIC density profiles are then compared with profiles from other diagnostics measuring the edge and SOL such as the lithium beam and Thomson scattering.

As measurements are performed at different poloidal locations, profiles have to be mapped for instance to normalized coordinates. After the mapping procedure, data from the different diagnostics

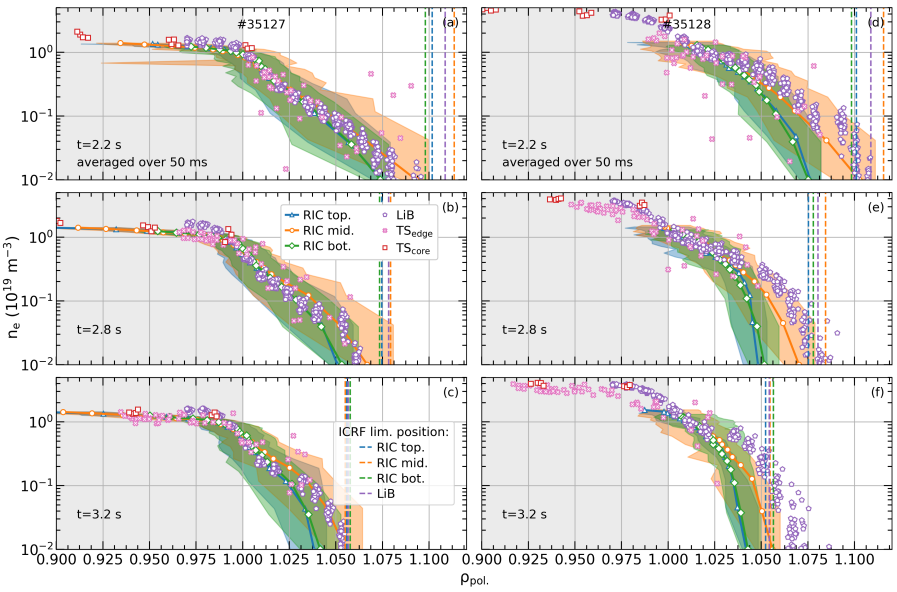

Figure 2. Electron density profiles obtained from RIC, LiB, edge and core TS diagnostics, for discharges #35127 (left column) and #35128 (right column) for three values of outer wall clearance. All the profiles are averaged over 50 ms. The shaded area of the reflectometry systems represents the variation of the profiles during the averaging period. The positions of the ICRF limiter at the RIC antenna top./mid./bot. and LiB locations are also indicated.

often appear to be radially displaced, most probably due to the uncertainties associated with each diagnostic and because the equilibrium may be nonaxisymmetric. It is a common practice to radially

shift profiles from different diagnostics in order to make the data consistent using the two-point model to estimate the separatrix temperature (e.g. [15]). However, for the low temperature expected for the separatrix in Ohmic discharges (30-40 eV) the two point model results in large uncertainties in the determination of the separatrix position due to the significant error bars in the TS data at this temperature range. Alternatively, the density measured by the edge interferometer is used here to align the density profiles. The TS and LiB density profiles are integrated along the line-of-sight of the edge interferometer with the profiles shifted to match the interferometry measurements. Then, RIC profiles are shifted in such a way that the averaged profiles (over 50 ms) fit TS and LiB data.

The electron density profiles from RIC, TS and LiB are shown in figure 2 for the low and high density discharges and for time periods corresponding to different outer wall clearances. The applied radial shifts are presented in table 1. At low discharge density (see left column in figure 2), a good agreement is observed between the different diagnostics in the SOL although the LiB tends to show a higher density inside the separatrix. The required shifts between the different diagnostics are in general small, in the order of 5 mm. The profile differences between the three RIC antennas might be due to poloidal density asymmetries but are more likely associated with uncertainties in the magnetic reconstructions. RIC antennas are located at different toroidal locations and for instance the toroidal field ripple is not taken into account in the magnetic reconstructions. This will be the subject of future work.

At high density (see right column in figure 2), RIC profiles tend to be steeper than LiB profiles in the near SOL, particularly at low clearance, not showing any evidence of a density shoulder. The disagreement observed between LiB and RIC profiles in the far-SOL may be explained by the scraping-off effect of the ICRF antenna as the RIC measurements are performed in front of the ICRF antenna contrary to those from LiB. This evidence is clearly seen in figure 2 (f), where LiB density profile goes beyond the ICRF limiter positions. At high discharge densities, large filaments are observed in the far-SOL just in front of the RIC antenna, which might be a cause for a larger radial shift in the RIC profiles. In addition, an enhanced scattering of the probing waves caused by filaments might affect the reflected signals, and, thus, the reconstructed profiles. Further studies on the mentioned effects are necessary.

4 Validation of the profile initialization

The variation of the RIC profiles position described in the previous section (see table 1), results probably from the uncertainties in the estimation of f_{FF} and the inexact assumption of a constant $n_{\mathrm{e},0}$. A validation of both parameters is therefore required.

4.1 Determination of the first fringe

The first fringe frequency f_{FF} is equal to the probing frequency corresponding to the rise in the amplitude of the reflected signal (see section 3). The time traces of the RIC top-plane antenna amplitude, averaged over 10 ms, of each probing frequency are shown in figure 3 in color mapped panels. The f_{ce} at the separatrix (green curve) and at the ICRF antenna limiter (pink curve) are the boundary limits for the FF detection algorithm [4]. The white line represents estimated f_{FF}. In spite of large variation in the plasma position during the discharge (also seen in the movement of the f_{ce} at separatrix), the FF remains roughly constant and is located in front of the ICRF limiter.

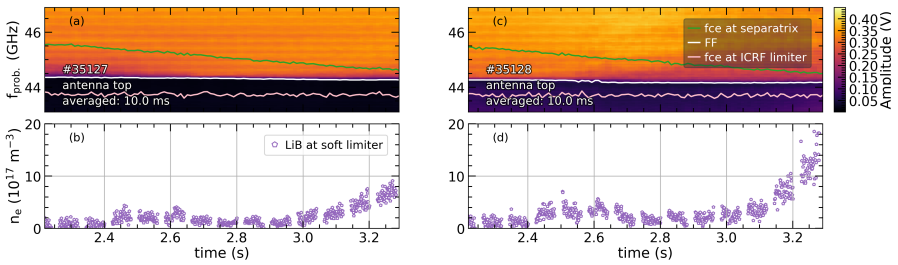

Figure 3. Top, time evolution of the reflected amplitude of the RIC top-plane antenna, for each probing frequency for discharges: (left) #35127, (right) #35128. The first fringe (FF, white curve) is estimated with the boundary limits at f_{ce} at separatrix (green curve) and f_{ce} at the ICRF limiter. Bottom, electron density estimated from LiB profile at the ICRF limiter position (soft limiter).

The reduction in the amplitude seen at high density low clearance (at the end of discharge #35128) is possibly due to scattering on density fluctuations and affects neither FF detection nor the profile reconstruction. No modulation of the amplitude is seen at low clearance (both for the low and high density discharges) suggesting that the impact of the plasma-wall multiple reflections is modest. As the FF occurs in front of the ICRF limiter, one can estimate the density at that location from the LiB data to confirm if the estimated residual is reasonable. As illustrated in the bottom panels of figure 3, the density in front of the ICRF limiter is always above or close to the residual density of RIC, confirming the RIC profiles initialize close to the ICRF limiter.

4.2 Residual density estimation

One can derive f_{ce} from (1.1): $f_{ce}(B) = \left(f_{UC}^2 - f_{pe}^2(n_e)\right)/f_{UC}$. Thus, assuming $f_{UC} = f_{FF}$ is known, changes in $n_{e,0}$ lead to different values of B, and therefore, to different initialization position. Instead of directly shifting the RIC profiles to match LiB profiles, as described in section 3, one can adjust the profiles varying $n_{e,0}$. Due to the difference in the profile shape of RIC and LiB, the adjustment cannot be performed on the whole profiles. Instead, the density ranges $0.5–0.75 \cdot 10^{18}\,m^{-3}$ and $0.9–1.2 \cdot 10^{18}\,m^{-3}$ were selected respectively for discharge #35127 and #35128. Density profiles were averaged (over 50 ms) and RIC profiles shifted to match the LiB profiles (previously shifted to fit edge interferometer as described in section 3) by adjusting $n_{e,0}$. Similarly, one can estimate the variation of $n_{e,0}$, using the standard deviation of LiB profiles in the averaging period. The evolution of the residual density as a function of the separatrix position at the outer middle plane for RIC top antenna is shown in figure 4. In the low density case (figure 4, left panel), $n_{e,0}$ slightly increases with the plasma position, resulting (as expected) in the outward movement of the profile. In high density case (figure 4, right panel), profiles need to be shifted inwards, thus the residual density is reduced. The standard deviation of LiB profiles is larger at high densities possibly due to changes in radial transport. Although $n_{e,0}$ varies with the discharge density and the plasma position, the dependence is rather weak. Therefore, as it is difficult to predict the value of $n_{e,0}$, it can be considered constant and in the order of $10^{17}\,m^{-3}$. For the wide range of experimental conditions tested here (large variation in the outer wall clearance and discharge density) $n_{e,0}$ is in the range $0.5–2 \cdot 10^{17}\,m^{-3}$, resulting in a variation of the profile initialization by about 1 cm.

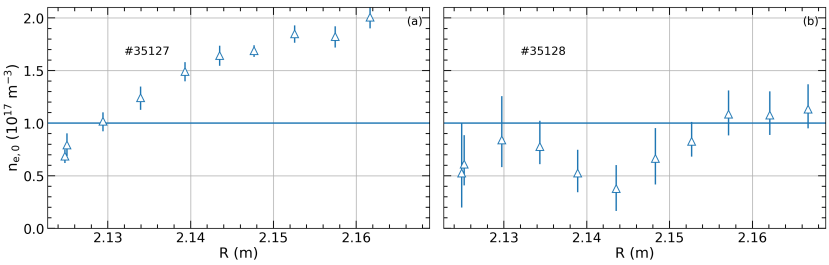

Figure 4. Dependence of the residual density, estimated from the fit of RIC top antenna profile to the LiB profile, averaged over 50 ms, on the separatrix position at the outer middle plane in (a) #35127, (b) #35128, corresponding to the period from 2.2 s to 3.2 s. The error bars correspond to the changes in the residual density due to variation of LiB profiles in the averaging period.

5 Conclusion

The density profiles from ICRF reflectometers, lithium beam emission spectroscopy and Thomson scattering systems have been compared in two discharges with a plasma position radial scan at low and high core densities, corresponding to low and high filamentary activity. The probing frequency corresponding to the start of X-mode upper cutoff reflection is generally observed just in front of the ICRF limiter. This can be implemented by initiating the profiles close to the limiter with a residual density that seems to be in the order of $n_{e,0} \approx 10^{17}$ m^{-3}. Apart from the observed discrepancy between the middle to the top and bottom antennas (which is possibly due to the accuracy of the equilibrium reconstruction), RIC profiles revealed a good agreement with SOL profiles obtained from LiB and TS in low density discharges. However, for high density discharges, RIC profiles tend to be steeper than LiB profiles in the near SOL, particularly at low clearance, not showing any evidence of a density shoulder. Full-wave simulations [16] will be applied to model the reflectometry diagnostic under different conditions of SOL turbulence, but focusing on the effects of filaments, with the physical understanding emerging from the simulations applied for a better understanding of the experimental profiles.

Acknowledgments

This work has been carried out within the framework of the EUROfusion Consortium and has received funding from the Euratom research and training program 2014–2018 and 2019–2020 under grant agreement No 633053. IST activities also received financial support from "Fundação para Ciência e Tecnologia" through project UID/FIS/50010/2019 and grants PD/BD/114326/2016 and PD/00505/2012 in the framework of the Advanced Program in Plasma Science and Engineering (APPLAuSE). The views and opinions expressed herein do not necessarily reflect those of the European Commission.

References

[1] D.E. Aguiam, A. Silva, V. Bobkov, P.J. Carvalho, P.F. Carvalho, R. Cavazzana et al., *Implementation of the new multichannel x-mode edge density profile reflectometer for the ICRF antenna on ASDEX upgrade*, *Rev. Sci. Instrum.* **87** (2016) 11E722.

[2] E. Mazzucato, *Microwave reflectometry for magnetically confined plasmas*, *Rev. Sci. Instrum.* **69** (1998) 2201.

[3] R.B. Morales, S. Hacquin, S. Heuraux and R. Sabot, *New density profile reconstruction methods in x-mode reflectometry*, *Rev. Sci. Instrum.* **88** (2017) 043503.

[4] D. Aguiam, *Implementation of a X-mode multichannel edge density profile reflectometer for the new ICRH antenna on ASDEX Upgrade*, Ph.D. thesis, Instituto Superior Técnico (2018).

[5] F. Clairet, C. Bottereau, J.M. Chareau, M. Paume and R. Sabot, *Edge density profile measurements by x-mode reflectometry on tore supra*, *Plasma Phys. Control. Fusion* **43** (2001) 429.

[6] S. Heuraux, F. da Silva and F. Clairet, *An X-mode reflectometry study on the reflection point for density profile reconstruction*, in *Proceedings of the 9th International Reflectometry Workshop*, Lisbon, Portugal, 4–6 May 2009.

[7] D.A. D'Ippolito, J.R. Myra and S.J. Zweben, *Convective transport by intermittent blob-filaments: Comparison of theory and experiment*, *Phys. Plasmas* **18** (2011) 060501.

[8] D. Carralero, G. Birkenmeier, H. Müller, P. Manz, P. deMarne, S. Müller et al., *An experimental investigation of the high density transition of the scrape-off layer transport in ASDEX upgrade*, *Nucl. Fusion* **54** (2014) 123005.

[9] M. Greenwald, *Density limits in toroidal plasmas*, *Plasma Phys. Control. Fusion* **44** (2002) R27.

[10] M. Willensdorfer, G. Birkenmeier, R. Fischer, F.M. Laggner, E. Wolfrum, G. Veres et al., *Characterization of the li-BES at ASDEX upgrade*, *Plasma Phys. Control. Fusion* **56** (2014) 025008.

[11] B. Kurzan and H.D. Murmann, *Edge and core thomson scattering systems and their calibration on the ASDEX upgrade tokamak*, *Rev. Sci. Instrum.* **82** (2011) 103501.

[12] H. Bottollier-Curtet and G. Ichtchenko, *Microwave reflectometry with the extraordinary mode on tokamaks: Determination of the electron density profile of petula-b*, *Rev. Sci. Instrum.* **58** (1987) 539.

[13] P. Varela, M. Manso, A. Silva, the CFN Team and the ASDEX Upgrade Team, *Review of data processing techniques for density profile evaluation from broadband FM-CW reflectometry on ASDEX upgrade*, *Nucl. Fusion* **46** (2006) S693.

[14] G. Wang, L. Zeng, E.J. Doyle, T.L. Rhodes and W.A. Peebles, *Improved reflectometer electron density profile measurements on DIII-d*, *Rev. Sci. Instrum.* **74** (2003) 1525.

[15] P.A. Schneider, L.B. Orte, A. Burckhart, M.G. Dunne, C. Fuchs, A. Gude et al., *Pedestal and edge localized mode characteristics with different first wall materials and nitrogen seeding in ASDEX upgrade*, *Plasma Phys. Control. Fusion* **57** (2014) 014029.

[16] F. da Silva et al, *Introducing REFMULF, a 2D full polarization code and REFMUL3, a 3D parallel full wave Maxwell code*, in *Proceedings of the 13th International Reflectometry Workshop*, Daejeon, South Korea, 10–12 May 2017.